Environmental Pollution 204 (2015) 145–151

Contents lists available at ScienceDirect

Environmental Pollution

journal homepage: www.elsevier.com/locate/envpol

Chloride-induced shape transformation of silver nanoparticles in a water environment

Lan Zhang [a, b], Xin Li [a], Rong He [b], Lijun Wu [a], Liyun Zhang [a, *], Jie Zeng [b]

[a] Institute of Technical Biology and Agriculture Engineering, Key Laboratory of Ion Beam Bioengineering, Hefei Institutes of Physical Science, Chinese Academy of Sciences, Hefei, Anhui 230031, PR China

[b] Hefei National Laboratory for Physical Sciences at the Microscale & Collaborative Innovation Center of Suzhou Nano Science and Technology, Center of Advanced Nanocatalysis (CAN-USTC) & Department of Chemical Physics, University of Science and Technology of China, Hefei, Anhui 230026, PR China

ARTICLE INFO

Article history:
Received 6 February 2015
Received in revised form
18 April 2015
Accepted 20 April 2015
Available online 14 May 2015

Keywords:
Silver nanoparticles
Environmental transformation
Chloride
Heterostructure
Water environments

ABSTRACT

The effects of chloride on dissolution and toxicity of silver nanoparticles (AgNPs) have been well studied. However, their intermediate shapes during the transition have not been illustrated to-date. Herein, the chloride-induced shape transformation process of AgNPs under long-term, low-concentration conditions is explored. A unique triangular Ag–AgCl heterostructure is observed. The structure then evolves into a symmetric hexapod and finally into a smaller AgNP. This transformation process could be affected by other environmental conditions, such as 0.4 mg/mL humic acid, 5% surfactants and 1 mg/mL bovine serum albumin protein. Our results offer new knowledge regarding the shape transformation process of AgNPs in the presence of chloride, which can be valuable in relevant studies concerning the effect of water chemistry on the behavior of AgNPs.

1. Introduction

Due to their inherent antimicrobial properties, silver nanoparticles (AgNPs) are widely used in a variety of products, including textiles, bandages, deodorants, baby products, toothpaste, air filters and household appliances (El-Temsah and Joner, 2012; Kumari et al., 2009). The increasing number of products containing AgNPs will lead to a larger release of AgNPs into the environment during the manufacture, use, cleaning and disposal of the products (Chen et al., 2013). This release could cause a mass interaction between AgNPs and many environmental factors (inorganic anions, metal cations, and even natural organic matters), leading to alterations in the composition, structure, and surface properties of the AgNPs (Chambers et al., 2013; Levard et al., 2013a, 2013b; Liu et al., 2013; Ma et al., 2013; Wirth et al., 2012). Accordingly, these alterations could in-turn affect the toxicity and transportation of AgNPs in natural water. Therefore, the environmental transformations of AgNPs should be investigated to determine their changes in morphology and size. However, many of the former toxicity studies that have been conducted regarding AgNPs are not environmentally relevant (Burchardt et al., 2012; Poynton et al., 2012; Schultz et al., 2012; van Aerle et al., 2013; Yu et al., 2013). The shape transformations of the nanoparticles under various environments conditions have been scarcely evaluated. In particular, knowledge of the intermediate products during the transforming process, which significantly affects the stability of AgNPs and consequently their bioavailability and toxicity, is limited.

Structurally, well-defined silver nanoparticles include nanospheres, nanocubes, nanoplates, nanoprisms, nanorods, nanowires and nanobelts, *etc.* (Jana et al., 2001; Jin et al., 2003, 2001; Liu et al., 2009; Sun et al., 2003; Zhang et al., 2009), yet most of these shapes are not thermodynamically stable in the presence of certain etching agents and tend to develop into new morphologies with lower surface free energies (An et al., 2008). This instability offers a great opportunity to utilize nanocrystals as environmental tracers by studying their transformation process under environmental exposure. Here, we chose Ag triangular nanoplates (Ag-TNPs) with relatively sharp corners as a typical example to demonstrate the susceptibility of AgNPs to environmental transformations based on the well-established localized surface plasmon resonance (LSPR) of Ag-TNPs (Jin et al., 2001; Kelly et al., 2003).

Ag triangular nanoplates, which exhibit striking color changes during structural transformations, along with the intrinsic strong

* Corresponding author.
E-mail address: zly0605@ustc.edu.cn (L. Zhang).

http://dx.doi.org/10.1016/j.envpol.2015.04.018
0269-7491/

in-plane dipole resonance, have been explored as indicators to visually depict shape conversion, which can be utilized in long-term research with low-concentration exposure to various environments. The interactions between Ag-TNPs and anions, which extensively exist in natural environments, have been widely investigated (An et al., 2008; Cathcart et al., 2009; Hou et al., 2014; Hsu et al., 2010; Jiang and Yu, 2008; Yang et al., 2013). For example, researchers have found that Cl^- can etch the corners and side faces of the Ag-TNPs, resulting in the transformation of Ag-TNPs to disk-like shapes (An et al., 2008). Further studies have shown that in addition to Cl^-, anions such as Br^-, I^-, $H_2PO_4^-$, and SCN^- can also interact with Ag-TNPs and shift the SPR band of the Ag-TNPs. Therefore, Jiang and Yu demonstrated a simple sensing method to detect inorganic anions by SPR shifts of Ag-TNPs (Jiang and Yu, 2008). Huang's group studied the time-dependent surface plasmon resonance spectroscopy of silver TNPs in the presence of halide (Hsu et al., 2010). However, from an environmental point of view, the long-term, low-concentration and multi-factor co-exposure are far different from the chemical contexts, and therefore, further environmentally-relevant studies are required. This work explores the shape transformation of Ag-TNPs in a water environment using LSPR and transmission electron microscopy (TEM), with an emphasis on the intermediate stages during the environmental transformation process. In addition, a systematic evaluation of the shape transformations and environmental fates of Ag-TNPs mediated by environmental factors are illustrated in this study, which are valuable for expanding our knowledge of the effect of water chemistry on the behavior of AgNPs.

2. Materials and methods

2.1. Materials

Silver nitrate ($AgNO_3$), L-ascorbic acid (AA), sodium citrate (Na_3CA), sodium borohydride ($NaBH_4$), poly(vinyl pyrrolidone) (PVP, MW ≈ 29,000), and potassium chloride (KCl) were purchased from Sinopharm Chemical Reagent Co. Lid. (Shanghai, China). Humic acid (HA), sodium dodecyl sulfate (SDS), tween 20, triton X-100, bovine serum albumin (BSA) and 11-mercaptoundecanoic acid (11-MUA) were purchased from Sigma–Aldrich. All of the chemicals were used as received without further purification. Ultrapure Millipore water (18.2 MΩ cm) was used as the solvent throughout.

2.2. Preparation of Ag triangular nanoplates

The Ag nanoplates were prepared using a previously reported seed-mediated procedure (Zeng et al., 2010, 2011). Two steps were involved. In the first step, Ag seeds were prepared as follows: 0.3 mL of aqueous $NaBH_4$ (5 mM) was injected into an 11-mL aqueous solution containing $AgNO_3$ (0.11 mM) and Na_3CA (2.05 mM) under magnetic stirring. Stirring was stopped after 10 min. This seed solution was then aged at room temperature for 5 h prior to use. In the second step, 100 mL of ultrapure water was mixed with aqueous $AgNO_3$ (2.5 mL, 5 mM), aqueous PVP (7.5 mL, 0.7 mM), aqueous Na_3CA (7.5 mL, 30 mM), and the as-prepared seed solution (0.2 mL), followed by slow dropping into aqueous AA (62.5 mL, 1 mM) under magnetic stirring. The color of the solution gradually changed into cyan. The product was directly used for the environmental shape transformation tests without further purification or treatment.

2.3. Instrumentation

TEM images were taken using a Hitachi H-7650 transmission electron microscope at an acceleration voltage of 100 kV. The UV–Vis–NIR extinction spectra were obtained using a Shimadzu UV-VIS-NIR spectrophotometer (UV-3600). The concentration of Ag-TNPs was determined via inductively coupled plasma atomic emission spectroscopy (ICP-AES, Atomscan Advantage, Thermo Jarrell Ash Corporation, USA). The X-ray photoelectron spectra (XPS) analysis was performed using an ESCALAB 250 (Thermo-VG Scientific). The specimens for XPS were prepared by covering the Ag–AgCl hybrid nanoplates on silicon wafers. The X-ray diffraction (XRD) analysis was performed using a MiniFlex 600 (Rigaku). The specimens for XRD were prepared by covering the Ag–AgCl hybrid nanoplates on glass sheets.

2.4. Shape transformation studies of the Ag triangular nanoplates under various environmental conditions

Using a standard procedure for the chloride-induced Ag-TNP shape transformation experiment, 10 or 20 portions of 0.1 mL KCl solution was added to 25 mL of the aqueous suspension of triangular Ag nanoplates (500 ng L^{-1} determined by ICP-AES, pH 6.8) during each titration under magnetic stirring. The reaction was quenched at a specific time point via centrifugation at 12,000 rpm for 5 min. The product was then precipitated twice with 10 mL water via centrifugation and decantation. The final product was re-dispersed in water for further structural analyses and UV–Vis–NIR measurements. For the reactions involving other environmental factors, the Ag nanoplates were incubated with the different environmental factors (HA, surfactants, protein, and thiol) in a vial for 24 h before the addition of KCl. A similar procedure was used. The typical resolution of the time course spectra that were recorded every 2 min was approximately 1 nm under constant Cl-ions concentration. All experiments were repeated at least three times.

3. Results and discussion

3.1. Properties of the Ag triangular nanoplates (Ag-TNPs)

The synthesized Ag-TNPs were characterized based on TEM and the UV–Vis–NIR extinction spectrum. As shown in the TEM image, the Ag-TNPs exhibit an average thickness of approximately 5 nm and with edge lengths varying in the range of 70–80 nm (Fig. 1 and Fig. S1). The Ag-TNPs display three distinct peaks at 332 nm, 555 nm and 804 nm (Fig. 1). According to previous studies, the small, sharp peak at 332 nm is attributed to the out-of-plane quadrupole SPR band of the Ag-TNPs. The peaks centered at 555 nm and 804 nm are attributed to the in-plane quadrupole and

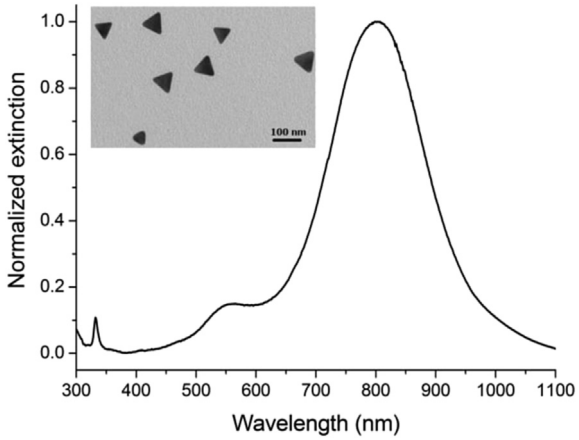

Fig. 1. UV–Vis–NIR extinction spectrum and TEM image of Ag-TNPs (inset).

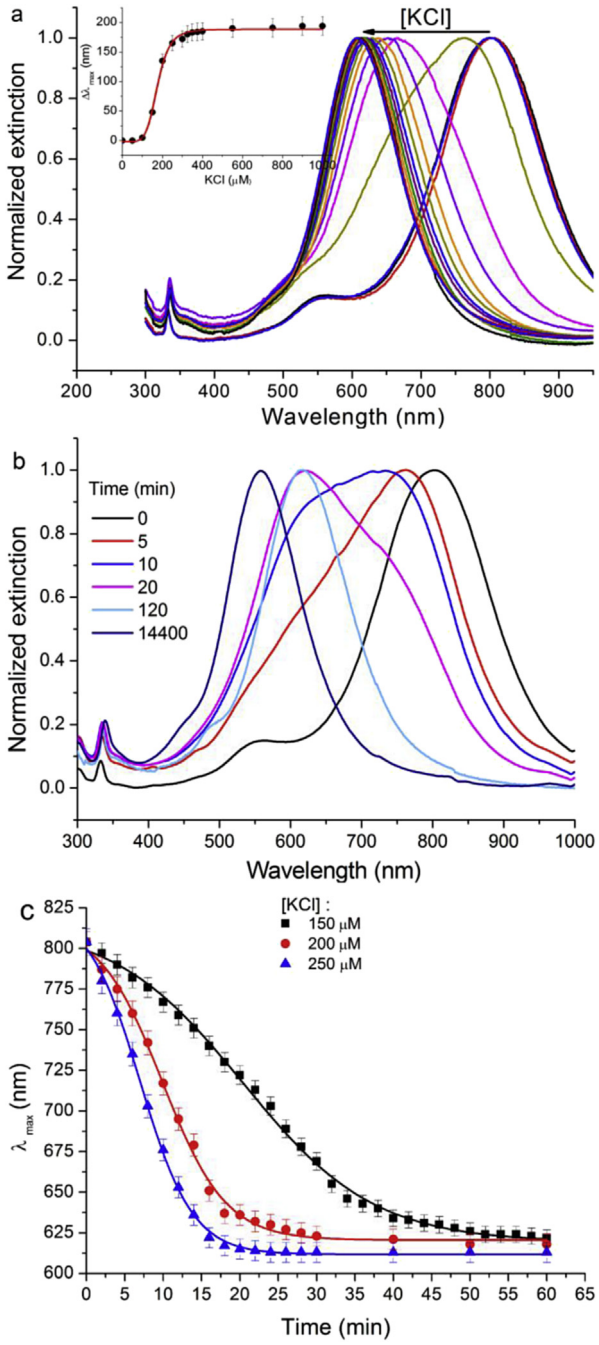

Fig. 2. (a) Extinction spectra of the Ag-TNP colloids in the presence of various concentrations of KCl for 15 min. The inset shows the blue-shift wavelength of the in-plane dipole SPR of the Ag-TNPs versus the concentration of KCl after 15 min. (b) The extinction spectra of the Ag-TNPs in the presence of 250 μM KCl for various durations of elapsed time. (c) The peak position of the in-plane dipole SPR versus the time after KCl addition.

dipole SPR bands of the Ag-TNPs, respectively (Kelly et al., 2003). The clear appearance of the three peaks confirms that the Ag-TNPs are highly uniform in both size and shape.

3.2. Chloride-induced Ag-TNP shape transformation

Chloride (Cl^-) is a ubiquitous anion in natural water (typical concentrations found in freshwater and seawater are 0.01 and 0.5 M, respectively) (Levard et al., 2012). In the natural environment, AgNPs may be present at a relatively low concentrations compared to laboratory conditions. The total amount of silver in environmental water samples has been reported to be in the range of one to hundreds of ng L^{-1} (Kramer, 1993), whereas in most chemical contexts, a higher AgNPs colloid concentration has been applied, such as 10 mg L^{-1} (An et al., 2008). In our study, to simulate the environmental conditions, the concentration of Ag-TNPs colloids was applied in the nanomolar scale (500 ng L^{-1}). Fig. 2 shows the UV–Vis–NIR extinction spectra of the Ag-TNPs in the presence of various concentrations of KCl. These UV–Vis–NIR spectra show that the in-plane dipole SPR blue shifted from 804 to 608 nm, whereas the out-of-plane quadrupole SPR slightly red shifted from 332 nm to 336 nm after the addition of 1 mM KCl for 15 min. The red-shift of the out-of-plane SPR bands and the blue-shift of the in-plane SPR bands indicate a decrease in the aspect ratio (the ratio of edge length to thickness) of the Ag-TNPs. We discovered that there was a threshold concentration (100 μM) of Cl^- ions to initiate the shape transformation (Fig. 2a). Over the KCl threshold concentration, such as at 150 μM, the shape-transformation process was time-dependent (Fig. 2, b and c). In addition, the LSPR spectra displayed a series of transitional evolutionary processes. The position of the in-plane dipole SPR shows blue shift from 804 nm to 558 nm after ten days of reaction. Fig. 2b shows the shape transformation process as time progressed based on the UV–Vis–NIR spectra in the presence of 250 μM KCl. The widening of the in-plane dipole SPR and the disappearance of the in-plane quadrupole SPR implied that the shape evolutions underwent several major intermediate products. The peak position (λ) of the in-plane dipole SPR peak displayed concentration- and time-dependent behavior (Fig. 2c). The effect of Cl^- on the shape transformation process may be codified in terms of kinetic parameters relevant to their processes, which can be obtained by fitting the data. Chloride-induced Ag-TNP shape transformation kinetics can be described by a sigmoidal curve defined by its initial shape, the subsequent transformation and its final equilibrium shape. Independent of the Cl^- concentration, experimental data are fit well by such a sigmoidal curve, as given in Equation (1) (Linse and Linse, 2011),

$$\lambda = \frac{\lambda_1 - \lambda_2}{1 + e^{(t-\tau)k}} + \lambda_2 \quad (1)$$

where λ is the peak position of the in-plane dipole SPR at time t, λ_1 and λ_2 are the initial and final stable peak positions, respectively, τ is the time required to reach half the final position, and *k* is the apparent first-order transformation constant. All data are listed in Table S1. Based on these results, the chloride-induced Ag-TNP shape transformation is a pseudo first-order process. The value of *k* indicates the rate of the transformation, which is a concentration-dependent parameter. However, when Cl^- is at a relatively high concentration (such as 0.5 M, which is a typical concentration in seawater), the reaction rate is too fast, and thus, the time-dependent behavior cannot be feasibly recorded using a commercial UV–Vis–NIR spectrometer. At excessively small amounts of Cl^- below or even near the threshold concentration, the kinetic process cannot be determined. Therefore, the application of Equation (1), used to analyze the shape transformation kinetic process, is limited to moderate Cl^- concentrations. Differentiating Equation (1) by t and subsequently rearranging yields:

$$\frac{d\lambda}{dt} = k\frac{1}{(\lambda_2 - \lambda_1)}(\lambda_2 - \lambda)(\lambda - \lambda_1) \quad (2)$$

where λ_2 is tentatively determined as t(∞). The shape transformation begins at λ_1 and finally stabilizes at the λ_2 position.

Equation (2) is a logistic differential equation and clearly shows that the above-described sigmoidal curve is a logistic curve for our experimental results. The Equation (2) may imply that Cl^- could function as a stabilizing agent. The long-term transformation process is tracked using LSPR (Fig. S2), as demonstrated by the disappearance of the blue shift after several months. Previous studies have also reported similar stabilization of Cl^- (An et al., 2008; Im et al., 2005). However, other stabilizing agents, such as PVP, which is included in the synthesis, are still present on the surface of the nanostructures after the exposure to chloride. Therefore, the capping agents and chloride are likely responsible for the stability of the newly formed disk-like structures. Huang et al. explained that the change in peak positions of the in-plane dipole SPR of silver colloids in the presence of Cl^- ions are correlated to the truncating effect on the corners of the silver nanoplates and to the increase in the nanoplate thickness (Hsu et al., 2010). However, a thickness change was not observed in our data (Fig. S3). Therefore, a new mechanism regarding the role of Cl^- in shape transformation must be proposed.

3.3. Tracking the chloride-induced Ag-TNP shape transformation process

LSPR spectra suggest an evolution of the morphology of the Ag-TNPs with time (Fig. 2b). To further explore the shape transformation process of Ag-TNPs in presence of Cl^- ions, TEM was used to track the intermediate products over a short time by quenching the reaction at different time points in addition to after the long-term process. These intermediate products have been largely ignored in previous studies (An et al., 2008; Hsu et al., 2010; Jiang and Yu, 2008). We demonstrated that elemental silver was sensitive in air-saturated water. Under oxygenated conditions, Ag^0 on the nanoparticle surface is oxidized to Ag^+ (Liu and Hurt, 2010). Thus, in presence of Cl^- ions, the reaction can be described by Equation (3) (Li et al., 2010), as follows.

$$4Ag + 4Cl^- + O_2 + 2H_2O \rightarrow 4AgCl + 4OH^- \quad (3)$$

Based on the solubility constants ($K_{sp,AgCl} = 1.76 \times 10^{-10}$) (Jiang and Yu, 2008), AgCl spontaneously forms when elemental Ag^+ and Cl^- encounter one another, which accelerates the oxidation of Ag^0. Fig. 3, a-e shows TEM images of the original triangular nanoplates of Ag and a series of intermediate products collected at different time points. The chloride-induced Ag-TNP shape transformation was selectively initiated at the corners of a triangular nanoplate, which progressed toward the central region (Fig. 3, b and c). The Ag–AgCl hybrid nanoplates in the initial stage of the shape transformation had a similar structure to a reported Ag–Ag_2S heterostructure (Zeng et al., 2011). As the reaction time expanded, the AgCl parts transited into a hexapod structure (Fig. 3d). However, the hexapod structure was unstable under irradiation and even in air (Fig. S4). Consequentially, the hexapods tended to shrink into disk-like nanoplates (Fig. 3e). Here, for the first time, we observed a hexapod structure in the AgCl–Ag system.

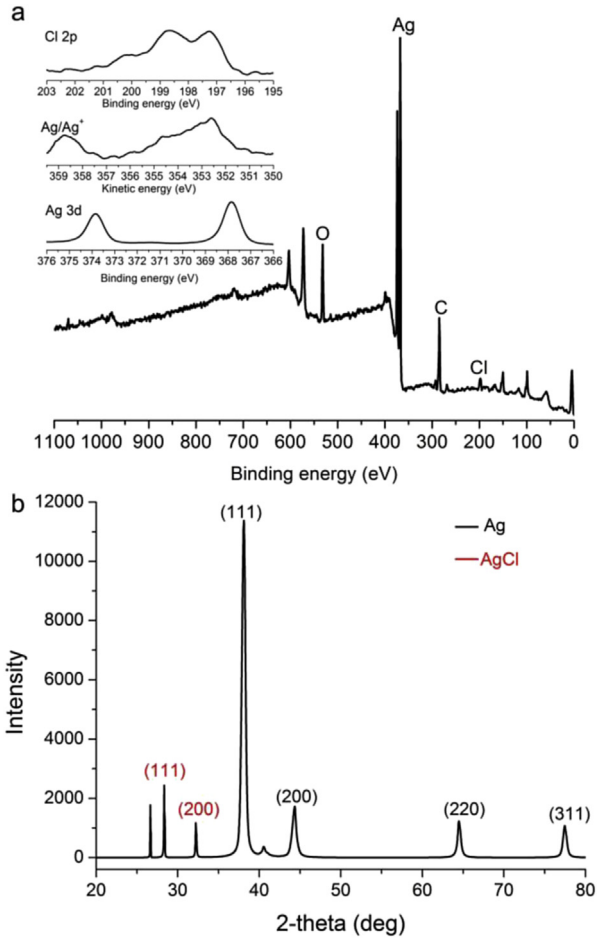

Fig. 4. (a) XPS survey scan of Ag–AgCl heterostructures and high resolution XPS spectra of Cl 2p (top inset), auger kinetic energy of Ag in Ag–AgCl heterostructures (middle inset) and Ag 3d peaks (bottom inset). (b) XRD pattern of Ag–AgCl heterostructures. The positions of the Ag and AgCl references were taken from the JCPDS database (Ag: 04-0783, AgCl: 06–0480).

To analyze composition on the surface of the Ag–AgCl heterostructure, XPS was used as a surface-sensitive technique to probe

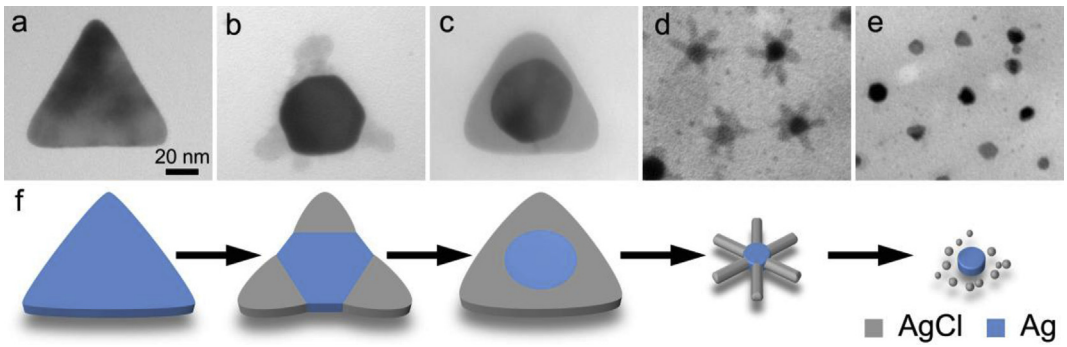

Fig. 3. (a) TEM image of the original Ag triangular nanoplates. (b–e) TEM images of the products obtained after the transformation had progressed for (b) 20 min, (c) 120 min, (d) 30 days and (e) 50 days. The dark region in the center corresponds to Ag, and the gray regions at corner sites correspond to AgCl. The scale bar in (a) is 20 nm and applies to all TEM images. (f) Schematic illustration of the shape transformation process by which elemental Ag reacts with Cl-.

the AgCl in the state corresponding to Fig. 3c, in which an Ag–AgCl heterostructure was observed. The XPS survey scan showed peaks indicating the presence of Ag and Cl from the nanoparticles and C and O from the capping reagent (Fig. 4a). High-resolution scans were performed in the binding energy range of the Cl and Ag peaks: Cl 2p and Ag 3d (Fig. 4a, inset). Cl 2p near 200 eV was present in the XPS spectra, suggesting the existence of AgCl (Fig. 4a). The chemical state of Ag in the Ag–AgCl heterostructure was investigated via XPS. The auger kinetic energy of the Ag in Ag–AgCl heterostructure is displayed in the middle inset of Fig. 4a. The binding energies of Ag $3d_{5/2}$ and Ag $3d_{3/2}$ were 367.85 eV and 373.85 eV, respectively. However, it was difficult to identify the silver valence state due to the subtleness of chemical shift in the silver binding energy. Fortunately, the silver valence state was confirmed through the auger parameter. The auger kinetic energies of the silver in the Ag–AgCl heterostructure were 352.60, 354.65 and 358.70 eV. Therefore, the auger parameters of the silver in the Ag–AgCl heterostructure were calculated as 720.50, 723.5 and 726.55 eV. The silver in the Ag–AgCl heterostructure was confirmed to exist as Ag^+ and Ag^0 (Kaushik, 1991). The XRD patterns of the Ag–AgCl heterostructure exhibited characteristic diffraction peaks associated with the structure of Ag and the structure of AgCl (Fig. 4b), which clearly revealed the formation of an Ag–AgCl heterostructure. This heterostructure can be interpreted through phase contrast changes on the same nanoparticles in the TEM images shown in Fig. 3.

Chloride ions are a significant factor influencing the properties of AgNPs including dissolution, aggregation, and toxicity, which have been investigated extensively (Im et al., 2005; Schultz et al., 2012; van Aerle et al., 2013; Zeng et al., 2011). Additionally, previous studies revealed that Cl^- can act as an etchant to manipulate the morphology of AgNPs from triangular plates with sharp corners to disk-like plates (An et al., 2008). However, to date, no clear mechanism depicts this transformation process. In our study, for the first time, we identified several significant intermediate structures, including Ag–AgCl triangular and hexapod heterostructures, by tracking the transformation procedure. The procedure can be described as follows: first, Cl^- ions diffuse into the lattice of Ag atoms where the triangular shape is essentially preserved; then, Ag–AgCl triangular nanoplates transform into hexapods; finally, the hexapod Ag–AgCl heterostructures lose the AgCl part and form shrunken disk-like nanoplates (Fig. 3f).

3.4. Effects of other environmental factors on chloride-induced Ag-TNP shape transformation

To explore how the other factors affect the chloride-induced Ag-TNP shape transformation process in water environments, subsequent experiments were performed.

3.4.1. Humic acid (HA)

Humic acid makes up an important fraction of natural organic matter and has been reported as a reducing and capping agent under environmentally relevant conditions and to further endow colloidal stability of AgNPs by preventing agglomeration (Akaighe et al., 2011). As shown in Fig. 5a, in the presence of 0.4 mg L^{-1} HA, the threshold concentration for Cl^- increased from 0.10 mM to 3.3 mM to induce Ag-TNP shape transformation, revealing that the chloride-induced Ag-TNP shape transformation process was impeded by HA. This impediment is also indicated from a reduction in the blue shift ($\Delta\lambda$) in SPR. To elucidate this finding, we carefully characterized the Ag-TNPs structures in the presence of both HA and Cl^- using TEM. As shown in Fig. S5, Ag-TNPs were stacked together face-to-face to form a self-assembled Ag superlattice in the presence of HA (Fig. S5a). More HA rendered increasingly tight stacking superlattices (Fig. S5d). Such

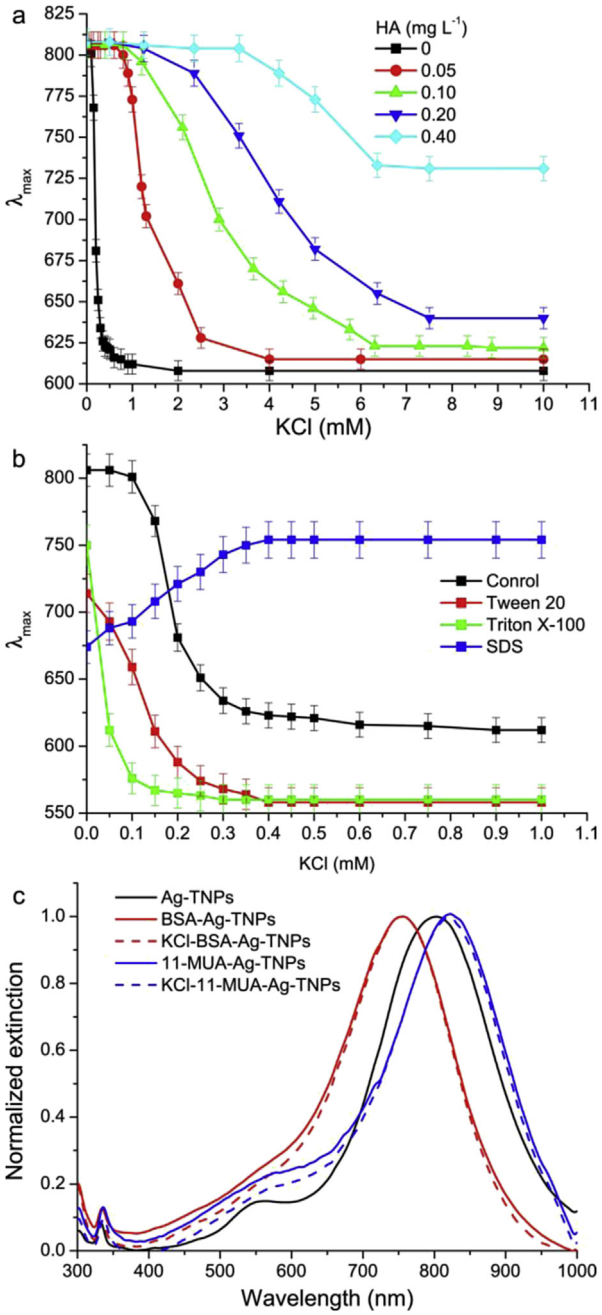

Fig. 5. (a) The position of the Ag-TNP in-plane dipole SPR in the presence of various concentrations of HA versus KCl. (b) The position of the Ag-TNP in-plane dipole SPR in the presence of 5% surfactants versus KCl. (c) Extinction spectra of Ag-TNPs modified with 1 mg/mL BSA or 11-mercaptoundecanoic acid (11-MUA) in the absence or presence of 20 mM KCl after 2 h.

Ag superlattices were stabilized by HA and hindered the chloride-induced Ag-TNP shape transformation (Fig. S5, b, e, and f). However, the hindrance of HA did not fundamentally prevent this transformation. As shown in Fig. S5c, for higher concentrations of Cl^- ions, the original Ag-TNPs finally transformed into smaller disk-like nanoplates. It is well known that two-dimensional nanocrystals (NCs) are unique materials that can assemble either face-to-face to form a thermodynamically favorable one-dimensional structure or edge-to-edge to form a planar two-dimensional structure (Hu et al., 2014). In a colloidal solution of Ag-TNPs, the predominant interactions of the nanoparticles are attributed to van der Waals forces, electrostatic forces and interactions between Ag-

TNPs and capping agents. The addition of HA may change the charges on the Ag-TNPs and the steric repulsion, thus promoting the self-assembly via van der Waals forces.

3.4.2. Surfactant

Surfactants are a diverse group of chemicals known for their wide use in detergents and other cleaning products. After use, residual surfactants are discharged into sewage systems or directly into surface waters, and most end up dispersed in various environmental compartments, such as soil, water and sediment. To assess the effect of the surfactants on chloride-induced Ag-TNP shape transformation, we selected SDS, tween 20, and triton X-100 as models. As shown in Fig. S6, the Ag-TNPs displayed a distinct in-plane dipole SPR blue shift ($\Delta\lambda$) of 84, 53 and 127 nm in 5% solutions of tween 20, triton X-100 and SDS, respectively. Cl^- ions reversed the blue shift in SDS solution. Although the chloride-induced shape transformation process still occurred in the solution of tween 20 and triton X-100. Further concentration-dependent experiments indicated that the shape transformation of the Ag-TNPs in the presence of non-ionic surfactants (tween 20 and triton X-100) occurred more easily when induced by Cl-ions (Fig. 5b). These results demonstrate that surfactants in the water environment impact the transformation of silver nanoparticles.

3.4.3. Biomacromolecule

It was previously reported that bovine serum albumin (BSA), a model protein, reduces the toxicity of AgNPs toward *nitrosomonas europaea* (Ostermeyer et al., 2013). In this study, we used BSA as a representative of biomacromolecule in environmental water. Fig. 5c shows the UV–Vis–NIR spectra of the as-prepared Ag-TNPs colloids modified by BSA before (red, solid line) and after (red, dashed line) the addition of 20 mM KCl for 2 h. As shown, the extinction spectra corresponding to the BSA-modified Ag-TNPs in 20 mM Cl^- ions are almost the same as the spectra recorded in the absence of Cl^-. The BAS-modified Ag-TNPs can endure a higher concentration of chlorine ions than the unmodified Ag-TNPs by at least 200-fold. It is clear that the presence of BSA restrains the chloride-induced shape transformation of the Ag-TNPs. This result is likely due to the presence of the sulfhydryl group in BSA, which may stabilize the structure of the Ag nanoplates (Lee et al., 2010). To further explore this mechanism, 11-mercaptoundecanoic acid (11-MUA) was chosen as a model to test the effect of the sulfhydryl group on the chloride-induced Ag-TNP shape transformation process. As shown in Fig. 5c, the extinction spectra remained the same before (blue, solid line) and after (blue, dashed line) the addition of KCl. This result demonstrated that the presence of sulfhydryl groups suppresses the chloride-induced Ag-TNP shape transformation.

4. Conclusions

The natural water environment is a complex system. Other environmental factors exert different influences on chloride-induced Ag-TNP shape transformation. Therefore, it is difficult to elucidate the environmental fate of Ag-TNPs. In this study, we show a unique shape transformation process of Ag-TNPs and demonstrate the effect of other environmental factors on the final fate of Ag-TNPs. These results are of value for expanding our knowledge of the intermediate products in the transformation process of a variety of nanoparticles. Compared to previous studies involving Cl^-, this process is tracked over the long-term using TEM, and the effects of both the reaction time and concentration of Cl^- are investigated in detail. We found that Cl^- reacts with Ag nanocrystals in the presence of oxidants, and consequently, an Ag–AgCl triangular heterostructure is formed. This Ag–AgCl triangular heterostructure further evolves into a symmetrical hexapod structure over the long-term reaction. Our studies also reveal that the hexapod structures are unstable under irradiation in water environments. These results offer new information on the environmental fate of AgNPs

Acknowledgments

This study was supported by MOST of China (Grant No. 2014CB932002), Natural Science Foundation of China (Nos. 11105150 and 51371164) and the Special Financial Grant from China Postdoctoral Science Foundation (No. 2013T60613).

Appendix A. Supplementary data

Supplementary data related to this article can be found at http://dx.doi.org/10.1016/j.envpol.2015.04.018.

References

Akaighe, N., MacCuspie, R.I., Navarro, D.A., Aga, D.S., Banerjee, S., Sohn, M., Sharma, V.K., 2011. Humic acid-induced silver nanoparticle formation under environmentally relevant conditions. Environ. Sci. Technol. 45, 3895–3901.
An, J., Tang, B., Zheng, X., Zhou, J., Dong, F., Xu, S., Wang, Y., Zhao, B., Xu, W., 2008. Sculpturing effect of chloride ions in shape transformation from triangular to discal silver nanoplates. J. Phys. Chem. C 112, 15176–15182.
Burchardt, A.D., Carvalho, R.N., Valente, A., Nativo, P., Gilliland, D., Garcìa, C.P., Passarella, R., Pedroni, V., Rossi, F., Lettieri, T., 2012. Effects of silver nanoparticles in diatom *Thalassiosira pseudonana* and cyanobacterium *synechococcus* sp. Environ. Sci. Technol. 46, 11336–11344.
Cathcart, N., Frank, A.J., Kitaev, V., 2009. Silver nanoparticles with planar twinned defects: effect of halides for precise tuning of plasmon resonance maxima from 400 to >900 nm. Chem. Commun. 7170–7172.
Chambers, B.A., Afrooz, A.R.M.N., Bae, S., Aich, N., Katz, L., Saleh, N.B., Kirisits, M.J., 2013. Effects of chloride and ionic strength on physical morphology, dissolution, and bacterial toxicity of silver nanoparticles. Environ. Sci. Technol. 48, 761–769.
Chen, S., Theodorou, I.G., Goode, A.E., Gow, A., Schwander, S., Zhang, J., Chung, K.F., Tetley, T.D., Shaffer, M.S., Ryan, M.P., Porter, A.E., 2013. High-resolution analytical electron microscopy reveals cell culture media-induced changes to the chemistry of silver nanowires. Environ. Sci. Technol. 47, 13813–13821.
El-Temsah, Y.S., Joner, E.J., 2012. Impact of Fe and Ag nanoparticles on seed germination and differences in bioavailability during exposure in aqueous suspension and soil. Environ. Toxicol. 27, 42–49.
Hou, X., Chen, S., Tang, J., Xiong, Y., Long, Y., 2014. Silver nanoplates-based colorimetric iodide recognition and sensing using sodium thiosulfate as a sensitizer. Anal. Chim. Acta 825, 57–62.
Hsu, M.-S., Cao, Y.-W., Wang, H.-W., Pan, Y.-S., Lee, B.-H., Huang, C.-L., 2010. Time-dependent surface plasmon resonance spectroscopy of silver nanoprisms in the presence of halide ions. Chemphyschem 11, 1742–1748.
Hu, C., Lin, K., Wang, X., Liu, S., Yi, J., Tian, Y., Wu, B., Chen, G., Yang, H., Dai, Y., Li, H., Zheng, N., 2014. Electrostatic self-assembling formation of Pd superlattice nanowires from surfactant-free ultrathin Pd nanosheets. J. Am. Chem. Soc. 136, 12856–12859.
Im, S.H., Lee, Y.T., Wiley, B., Xia, Y., 2005. Large-scale synthesis of silver nanocubes: the role of HCl in promoting cube perfection and monodispersity. Angew. Chem. Int. 44, 2154–2157.
Jana, N.R., Gearheart, L., Murphy, C.J., 2001. Wet chemical synthesis of silver nanorods and nanowires of controllable aspect ratio. Chem. Commun. 617–618.
Jiang, X.C., Yu, A.B., 2008. Silver nanoplates: a highly sensitive material toward inorganic anions. Langmuir 24, 4300–4309.
Jin, R.C., Cao, Y.C., Hao, E.C., Metraux, G.S., Schatz, G.C., Mirkin, C.A., 2003. Controlling anisotropic nanoparticle growth through plasmon excitation. Nature 425, 487–490.
Jin, R.C., Cao, Y.W., Mirkin, C.A., Kelly, K.L., Schatz, G.C., Zheng, J.G., 2001. Photoinduced conversion of silver nanospheres to nanoprisms. Science 294, 1901–1903.
Kaushik, V.K., 1991. XPS core level spectra and auger parameters for some silver compounds. J. Electron Spectrosc. Relat. Phenom. 56, 273–277.
Kelly, K.L., Coronado, E., Zhao, L.L., Schatz, G.C., 2003. The optical properties of metal nanoparticles: the influence of size, shape, and dielectric environment. J. Phys. Chem. B 107, 668–677.
Kramer, J.R.B.,G., 1993. Environmental Chemistry of Silver. SETAC Press, North Carolina.
Kumari, M., Mukherjee, A., Chandrasekaran, N., 2009. Genotoxicity of silver nanoparticles in Allium cepa. Sci. Total Environ. 407, 5243–5246.
Lee, B.-H., Hsu, M.-S., Hsu, Y.-C., Lo, C.-W., Huang, C.-L., 2010. A facile method to obtain highly stable silver nanoplate colloids with desired surface plasmon resonance wavelengths. J. Phys. Chem. C 114, 6222–6227.
Levard, C., Hotze, E.M., Colman, B.P., Dale, A.L., Truong, L., Yang, X.Y., Bone, A.J., Brown, G.E., Tanguay, R.L., Di Giulio, R.T., Bernhardt, E.S., Meyer, J.N.,

Wiesner, M.R., Lowry, G.V., 2013a. Sulfidation of silver nanoparticles: natural antidote to their toxicity. Environ. Sci. Technol. 47, 13440–13448.
Levard, C., Hotze, E.M., Lowry, G.V., Brown, G.E., 2012. Environmental transformations of silver nanoparticles: impact on stability and toxicity. Environ. Sci. Technol. 46, 6900–6914.
Levard, C., Mitra, S., Yang, T., Jew, A.D., Badireddy, A.R., Lowry, G.V., Brown, G.E., 2013b. Effect of chloride on the dissolution rate of silver nanoparticles and toxicity to *E. coli*. Environ. Sci. Technol. 47, 5738–5745.
Li, X.A., Lenhart, J.J., Walker, H.W., 2010. Dissolution-accompanied aggregation kinetics of silver nanoparticles. Langmuir 26, 16690–16698.
Linse, B., Linse, S., 2011. Monte Carlo simulations of protein amyloid formation reveal origin of sigmoidal aggregation kinetics. Mol. Biosyst. 7, 2296–2303.
Liu, B., Luo, W., Zhao, X., 2009. A facile synthesis of ordered ultralong silver nanobelts. Mater. Res. Bull. 44, 682–687.
Liu, J., Hurt, R.H., 2010. Ion release kinetics and particle persistence in aqueous nano-silver colloids. Environ. Sci. Technol. 44, 2169–2175.
Liu, Z.-h., Zhou, Y., Maszenan, A.M., Ng, W.J., Liu, Y., 2013. pH-dependent transformation of Ag nanoparticles in anaerobic processes. Environ. Sci. Technol. 47, 12630–12631.
Ma, R., Levard, C., Judy, J.D., Unrine, J.M., Durenkamp, M., Martin, B., Jefferson, B., Lowry, G.V., 2013. Fate of zinc oxide and silver nanoparticles in a pilot wastewater treatment plant and in processed biosolids. Environ. Sci. Technol. 48, 104–112.
Ostermeyer, A.-K., Kostigen Mumuper, C., Semprini, L., Radniecki, T., 2013. Influence of bovine serum albumin and alginate on silver nanoparticle dissolution and toxicity to *Nitrosomonas europaea*. Environ. Sci. Technol. 47, 14403–14410.
Poynton, H.C., Lazorchak, J.M., Impellitteri, C.A., Blalock, B.J., Rogers, K., Allen, H.J., Loguinov, A., Heckman, J.L., Govindasmawy, S., 2012. Toxicogenomic responses of nanotoxicity in daphnia magna exposed to silver nitrate and coated silver nanoparticles. Environ. Sci. Technol. 46, 6288–6296.
Schultz, A.G., Ong, K.J., MacCormack, T., Ma, G., Veinot, J.G.C., Goss, G.G., 2012. Silver nanoparticles inhibit sodium uptake in juvenile rainbow trout (Oncorhynchus mykiss). Environ. Sci. Technol. 46, 10295–10301.
Sun, Y.G., Mayers, B., Xia, Y.N., 2003. Transformation of silver nanospheres into nanobelts and triangular nanoplates through a thermal process. Nano Lett. 3, 675–679.
Van Aerle, R., Lange, A., Moorhouse, A., Paszkiewicz, K., Ball, K., Johnston, B.D., de-Bastos, E., Booth, T., Tyler, C.R., Santos, E.M., 2013. Molecular mechanisms of toxicity of silver nanoparticles in zebrafish embryos. Environ. Sci. Technol. 47, 8005–8014.
Wirth, S.M., Lowry, G.V., Tilton, R.D., 2012. Natural organic matter alters biofilm tolerance to silver nanoparticles and dissolved Silver. Environ. Sci. Technol. 46, 12687–12696.
Yang, X.-H., Ling, J., Peng, J., Cao, Q.-E., Ding, Z.-T., Bian, L.-C., 2013. A colorimetric method for highly sensitive and accurate detection of iodide by finding the critical color in a color change process using silver triangular nanoplates. Anal. Chim. Acta 798, 74–81.
Yu, S.j., Chao, J.b., Sun, J., Yin, Y.g., Liu, J.f., Jiang, G.b., 2013. Quantification of the uptake of silver nanoparticles and ions to HepG2 cells. Environ. Sci. Technol. 47, 3268–3274.
Zeng, J., Roberts, S., Xia, Y., 2010. Nanocrystal-based time-temperature indicators. Chem. - Eur. J. 16, 12559–12563.
Zeng, J., Tao, J., Su, D., Zhu, Y., Qin, D., Xia, Y., 2011. Selective sulfuration at the corner sites of a silver nanocrystal and its use in stabilization of the shape. Nano Lett. 11, 3010–3015.
Zhang, Q., Ge, J., Pham, T., Goebl, J., Hu, Y., Lu, Z., Yin, Y., 2009. Reconstruction of silver nanoplates by UV irradiation: tailored optical properties and enhanced stability. Angew. Chem. Int. 48, 3516–3519.